Available online at www.sciencedirect.com

ScienceDirect

J Materiomics 2 (2016) 25–36

www.ceramsoc.com/en/

www.journals.elsevier.com/journal-of-materiomics/

A review on one dimensional perovskite nanocrystals for piezoelectric applications

Li-Qian Cheng [a,b], Jing-Feng Li [a,*]

[a] State Key Laboratory of New Ceramics and Fine Processing, School of Materials Science and Engineering, Tsinghua University, 100084 Beijing, China
[b] Department of Materials Science and Engineering, China University of Mining & Technology, Beijing, 100083 Beijing, China

Received 22 November 2015; revised 1 December 2015; accepted 26 January 2016
Available online 17 February 2016

Abstract

In recent years, one-dimensional piezoelectric nanomaterials have become a research topic of interest because of their special morphology and excellent piezoelectric properties. This article presents a short review on one dimensional perovskite piezoelectric materials in different systems including $Pb(Zr,Ti)O_3$, $BaTiO_3$ and $(K,Na)NbO_3$ (KNN). We emphasize KNN as a promising lead-free piezoelectric compound with a high Curie temperature and high piezoelectric properties and describe its synthesis and characterization. In particular, details are presented for nanoscale piezoelectricity characterization of a single KNN nanocrystal by piezoresponse force microscopy. Finally, this review describes recent progress in applications based on one dimensional piezoelectric nanostructures with a focus on energy harvesting composite materials.

Keywords: Piezoelectric single crystals; Perovskite; One dimensional nanomaterials; Piezoresponse force microscopy; Piezoelectric applications

Contents

1. Introduction

Piezoelectric materials produce an electrical potential in response to an applied force or generate mechanical movement when subjected to an electric field [1–3]. Such smart materials have become essential for modern society, especially in the fields of information and communications, industrial automation, medical diagnostics, *etc.* [3]. Because of their scientific interests and rich applications, piezoelectric materials have attracted long-lasting attention from both academic and industrial communities for several decades with many recent exciting findings [4].

* Corresponding author.
E-mail address: jingfeng@mail.tsinghua.edu.cn (J.-F. Li).
Peer review under responsibility of The Chinese Ceramic Society.

http://dx.doi.org/10.1016/j.jmat.2016.02.003

Lead zirconate titanate, $Pb(Zr,Ti)O_3$, is a representative piezoelectric material, which has been widely used in many electronic devices. Alternative research seeks lead-free piezoelectric ceramics including $BaTiO_3$ and $(K,Na)NbO_3$ as well as $Bi_{0.5}Na_{0.5}TiO_3$ [5]. It is generally known that ferroelectric materials possess high piezoelectricity, and most of them are perovskite compounds with a common molecular formula of ABO_3. Thus, nanoscale ferroelectrics with a perovskite structure have been extensively studied in the last two decades with a focus on thin films because of their applications for memory devices and microelectromechanical systems (MEMS) [6]. Nevertheless, more and more studies have been recently devoted to perovskite nanostructures including nanowires, nanorods, nanotubes, nanobelts, nanowhiskers, nanoplates, which are expected to open up new applications in nanoelectronics and self-powered nanodevices [7–10]. Several good review articles have been published including that by Rørvik et al. who offered a detailed summary with an emphasis on processing techniques [6]. This short review will focus on one dimensional (1D) nanocrystals of some well-known perovskite ferroelectrics with more details about $(K,Na)NbO_3$ (KNN), which is a promising lead-free piezoelectric perovskite.

One dimensional nanocrystals have a high aspect ratio but a nanoscale cross-section with a width on the order of 100 nm [6]. Many methods have been developed for their synthesis, and interested readers can refer to the review by Rørvik et al. who presented a full view of processing progress that can be mainly categorized as template-assisted and template-free syntheses. There are many studies based on template-assisted synthesis using anodic aluminum oxide (AAO) and electrospinning method, but the materials fabricated by those two methods are generally polycrystalline [11–15]. We are more interested in nanoscale single crystals, and this review places emphasis on their fabrication processes including the molten salt reaction and hydrothermal methods [16–22].

One dimensional perovskite nanocrystals have interesting ferroelectric and piezoelectric properties, but few studies have characterized them. Piezo-response force microscopy techniques are powerful tools to measure the piezoelectric responses of an individual nanocrystal [23,24]. Several examples including our recent work on KNN nanocrystals will be reviewed here. Finally, this review will introduce some promising applications of piezoelectric sensors and energy harvesting devices.

2. Representative piezoelectric perovskites

Perovskites have a cubic structure with a general formula of ABO_3 as shown in Fig. 1. In this structure, the A-site ions are located on the corners of the lattice with B-site ions at body center positions; oxygen ions sit at face centers. An ideal perovskite with a cubic symmetry is not piezoelectric, but its distorted structures with non-cubic symmetries may possess good ferroelectricity and hence piezoelectricity. For example, in a perovskite with tetragonal symmetry as shown in Fig. 1, the B-site ions may shift downwards or upwards from the cubic body center resulting in a center asymmetric structure, which is a prerequisite for piezoelectric materials.

There are three classes of perovskite compounds including $A^IB^VO_3$, $A^{II}B^{IV}O_3$ and $A^{III}B^{III}O_3$ where the Roman numerals represent the chemical valence of cations (see Table 1). Recently, the lead-free piezoelectric KNN has become a good example of $A^IB^VO_3$ perovskites, which have an orthorhombic symmetry at room temperature. There are many examples of $A^{II}B^{IV}O_3$ perovskites, and the representative ones are $Pb(Zr,Ti)O_3$ and $BaTiO_3$. $A^{III}B^{III}O_3$ is also a good example. $BiFeO_3$ has attracted extensive attention as a multiferroic compound in addition to being a promising lead-free piezoelectric material [25]. Other well-known perovskites are listed in Table 1.

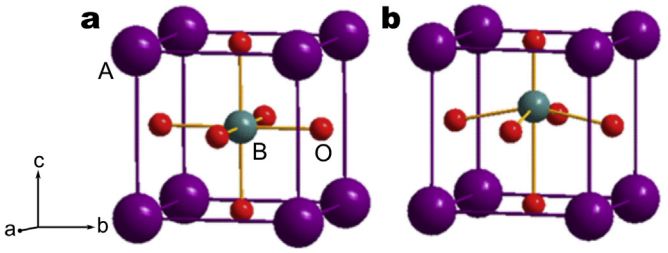

Fig. 1. Stereoscopic illustration of ABO_3 perovskite structure of (a) cubic and (b) tetragonal phase with polarization variants.

Table 1
Examples of perovskite structures.

Perovskite structures	System examples
$A^IB^VO_3$	$KNbO_3$, $NaNbO_3$, $(K,Na)NbO_3$
$A^{II}B^{IV}O_3$	$PbTiO_3$, $PbZrO_3$, $Pb(Zr,Ti)O_3$, $BaTiO_3$
$A^{III}B^{III}O_3$	$BiFeO_3$, $BiScO_3$

The most widely used piezoelectric materials are based on $Pb(Zr,Ti)O_3$ and commercially abbreviated as PZT. This is a solid solution of $PbZrO_3$ and $PbTiO_3$. There is a phase boundary between rhombohedral and tetragonal phases in the vicinity of the Zr/Ti = 52/48, which is known as morphotropic phase boundary (MPB) [5]. When the composition is adjusted close to the MPB, high piezoelectricity can be obtained because of enhanced polarization due to the phase co-existing effect. PZT-based materials are usually used in the form of ceramic bulks, which are fabricated by sintering process. Although single crystals outperform the sintered ceramics, it is difficult to grow PZT single crystals because compositional separation tends to occur during the crystallization. However, Pb is quite toxic and lead-free piezoelectric perovskites have a bright future.

$BaTiO_3$ (BTO) is a typical perovskite compound with an even longer history than PZT. It is now mainly used as a dielectric material for multilayered ceramic capacitors due to its low Curie temperature and low coercive field [26,27]. Nevertheless, great progress has been achieved in the development of $BaTiO_3$-based piezoelectric ceramics. $BaTiO_3$ has attracted continuous interest because of its simpler composition than PZT. There are many studies using $BaTiO_3$ as a model material to investigate the nanoscale effect of ferroelectrics [28]. It is

expected that more and more studies will be conducted about $BaTiO_3$ piezoelectric perovskite nanocrystals [29–33].

$(K,Na)NbO_3$ (KNN) is a promising lead-free piezoelectric material with higher Curie temperature even than PZT. A huge amount of research has been conducted on KNN-based ceramics in last decade leading to a great enhancement in piezoelectric charge coefficient from ~100 to ~500 pC/N [2,4,34]. Although the comprehensive properties of KNN based piezoelectric ceramics are still inferior to PZT counterparts, we believe that KNN is one of the most promising lead-free piezoelectrics. Synthesis of KNN nanocrystals is challenging because of its high alkalinity and easy evaporation of alkali oxides. However, its advantages of high piezoelectricity and high Curie temperature and the absence of lead toxicity have driven many studies including our own [34–41].

3. Synthesis of one dimensional perovskites

3.1. $PbTiO_3$ and PZT nanocrystals

The 1D piezo-nanocrystals containing Pb have high ferroelectric and piezoelectric performance values and are highly focused. Several kinds of synthesis approaches have been employed [42–49]. Of note, fabrication of $PbTiO_3$ (PT) nanocrystals has been studied even with more numbers of reports available in literature than PZT. This may be due to its compositional simplicity and higher spontaneous polarization.

Fig. 2 shows PT and PZT nanorods synthesized by molten salt and hydrothermal reactions, respectively [43,44,50,51]. The PT nanostrips shown in Fig. 2(a) were grown in the presence of NaCl/KCl mixed chlorides—this is known as the molten salt reaction. The width of PT nanostrips ranges from 20 nm to 100 nm, and their lengths reach tens of micrometers. The phase structures of the PT nanostrips are tetragonal as confirmed by X-ray diffraction [50]. Single-crystalline PT rods can also be obtained by the growth of PT nanocrystals, and the TEM image and selected area electron diffraction (SAED) of the products are shown in Fig. 2(b) [44]. For the hydrothermal synthesis, the PZT nanocrystals fabricated by a modified sol–gel method are used as seeds. The typical PZT nanorods shown in Fig. 2(c) were grown from the sol–gel-synthesized PZT nanocrystals that were added into the salt with appropriate surfactants. The mineralizer was also used in the hydrothermal synthesis of PZT nanorods in Fig. 2(c), and the morphology was modified by adjusting the mineralizer concentration and reaction time [43]. Moreover, the PZT rods shown in Fig. 2(d) were also obtained by a hydrothermal process assisted by surfactants [51]. The use of surfactants helps to suppress the radial growth of PZT particles leading to the formation of one dimensional structures.

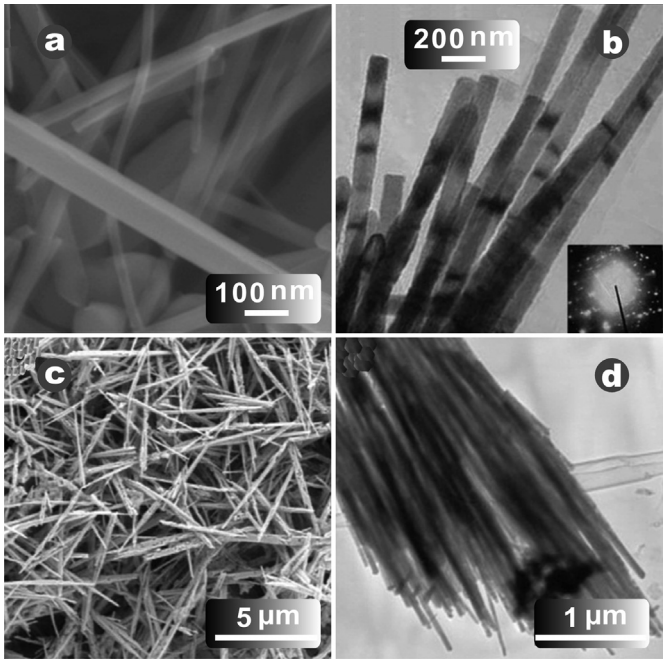

Fig. 2. PT and PZT nanorods synthesized by molten salt and hydrothermal methods. (a) SEM image [50] and (b) TEM image and SAED pattern of PT rods [44] fabricated *via* molten salt reaction. (c) SEM [43] and (d) TEM images of PZT nanorods with tetragonal phase [51] synthesized by hydrothermal process.

As discussed above, the molten salt method and hydrothermal reaction are employed in the synthesis of PT and PZT 1D nanocrystals, respectively. These two methods are considered to be template-free methods and are popular in syntheses of 1D piezo-nanocrystals due to the facile achievement of single crystalline nanostructures [38]. However, it is difficult to accurately determine the major processing parameters that affect the crystal growth [6]. Hu et al. reported that the competition between the supersaturation ratio and the surface energies of some nanostructures may lead products with various morphology and structures [52]. However, there are several parameters that affect the morphology and structures of 1D nanocrystals including the concentration of reactants, composition of solution, reaction temperature, surfactants, mineralizer, *etc.* It is interesting that the surfactants and mineralizer—which do not stay in the products—also play critical roles on the growth of 1D crystals. The surfactants include polyvinyl alcohol (PVA), polyacrylic acid (PAA), *etc.* [51], while the mineralizers include tetramethylammonium hydroxide pentahydrate (TMAH), *etc.* [43] leading to the anisotropic growth of the target products. Fig. 3 compares the growth of PT nanorods without and with surfactants through the molten salt reaction. The key mechanism for the product growth without surfactant is shown in Fig. 3(a) [50]. The PT nanoparticles first nucleate in the NaCl–KCl flux at a certain temperature, and then some little crystal seeds gradually aggregate preferentially along the one dimensional direction. They eventually evolve into a nanorod form. In the presence of surfactant (Fig. 3(b)), the fine particles steadily form nanorods along an axial direction due to the kinetic control of the surfactant shell [44].

Many studies have been conducted to fabricate the PT and PZT nanorod arrays [45,47,53,54]. Fig. 4 shows the aligned PT and PZT nanorod/microrod arrays grown on different substrates. For aligned growth, the substrate plays a pronounced effect on the orientation and configuration of rod arrays [53]. Of note, the epitaxial film layers in Fig. 4(a)–(d) are an essential component during the growth of rods, and the

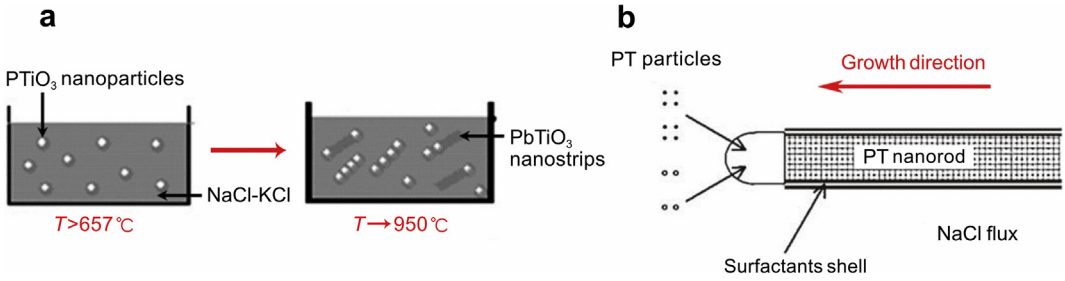

Fig. 3. Schematic illustration of the growth of PT nanorods fabricated *via* molten salt method (a) without [50] and (b) [44] with surfactant.

resulting rod arrays are all synthesized by the hydrothermal method. The rod array shown in Fig. 4(a) is aligned perpendicular to the substrate surface of a single crystalline $SrTiO_3$ substrate on which a PT film layer is grown [45]. The rods have a square cross-section of ~200 nm and are up to several micrometers long. The PT rods in Fig. 4(b) are grown on a ⟨100⟩ $SrTiO_3$ substrate, and seem to be parallel to the substrate. Actually, the PT nanorods grow perpendicular out of some platelet side surfaces, and upward from the platelet top surfaces. Some vertical rods are seen as white dots in the SEM image. In addition, the platelet is first synthesized as the initial products during the hydrothermal process [53]. The PZT rods shown in Fig. 4(c) and (d) are aligned on TiO_2 and (100) Nb−$SrTiO_3$ substrates, respectively. The TiO_2 substrate in Fig. 4(c) is a layer of TiO_2 formed on the surface of titanium foil by a thermal treatment at 600 °C in air as reported by Lin et al. [47]. The substrate and the hydrothermal solution were then placed in a stainless steel autoclave with a Teflon liner at 175 °C for 12 h. The SEM image clearly shows that the PZT rods are well aligned, and the diameter increases along the rod length from the bottom to the top [47]. Meanwhile, the diameter of rods in Fig. 4(d) is around 200 nm, and the length varies markedly [19]. The in-plane aligned PZT single crystal rod can also be grown on a $SrTiO_3$ substrate with gold particles on its surfaces by a simple method based on near migration and restricted growth process [54]. It is also a facile method to synthesize self-assembled PZT nanorods.

3.2. BTO nanocrystals

1D BTO nanostructures are lead-free piezomaterials and have received increasing attention both for their properties and applications [55]. The hydrothermal method is widely utilized in the fabrication of BTO nanostructures [33,56,57]. The SEM and TEM results of BTO nanorods—as well as the aligned BTO nanorod array—are shown in Fig. 5. Joshi et al. reported the template-free hydrothermal synthesis of BTO single crystals for the first time [33]. After that, hydrothermal methods became widely utilized in the fabrication of BTO 1D nanostructures. The BTO nanowires with high aspect ratios shown in Fig. 5(a) were effectively controlled by adjusting the hydrothermal reaction temperature [58]. The aspect ratios of BTO rods increased from 9.3 to 45.8 depending on the hydrothermal temperature. Fig. 5(b) shows a TEM image of BTO nanowires synthesized by a hydrothermal reaction [57]. The preparation of BTO nanowire arrays presented in Fig. 5(c) and (d) is based on a two-step hydrothermal reaction [59]. The diameter of the resulting rods is around 90 nm. The cross-sectional view of BTO nanowire array is also shown in Fig. 5, and the rods are aligned nearly vertically [31].

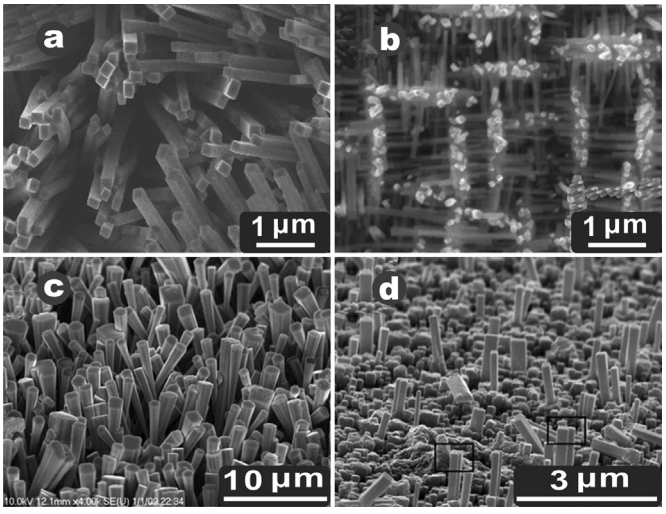

Fig. 4. Aligned PT and PZT nanorods/microrods grown on different substrates. (a) PT rod array on (001)-oriented PT substrate [45]. (b) PT rod array on (100)-oriented $SrTiO_3$ substrate [53]. (c) PZT wire array on the TiO_2 film formed on titanium substrate [47]. (d) PZT rod array on (100) Nb−$SrTiO_3$ substrate [19].

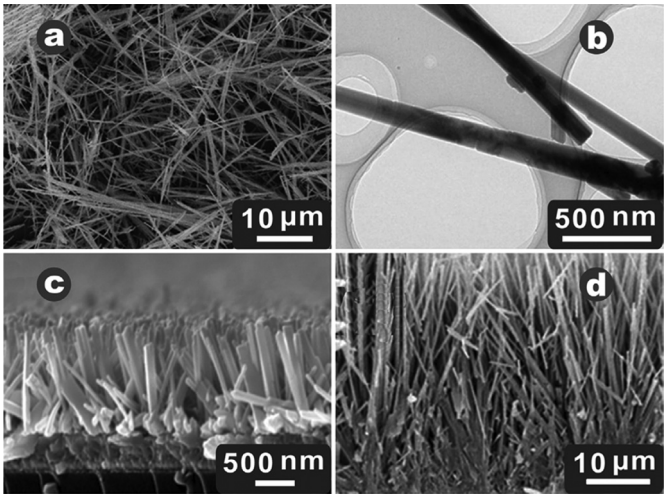

Fig. 5. BTO nanorods synthesized *via* hydrothermal methods. (a) SEM [58] and (b) TEM images [57] of BTO nanorods fabricated by a hydrothermal method. (c) Cross-sectional view of BTO nanorod array [59]. (d) The BTO nanowire array synthesized *via* a hydrothermal method [31].

The molten salt method can also be employed for the synthesis of BTO nanorods, however studies on the molten salt method are much less common than the hydrothermal method [29]. Mao et al. reported the fabrication of BTO nanorods *via* molten salt reaction as one of the pioneering works in 2003 [60]. More efforts have been made to improve the morphology and quality of BTO nanorods [50]. By using this molten salt synthesis method, Deng et al. studied the surfactant-free fabrication of BTO nanostrips as shown in Fig. 6(a) [50]. The BTO rods are straight and have a rectangular cross-section as seen from the low magnification SEM image. Their widths range from 50 to 200 nm (inset of Fig. 6(a)). Additionally, the TEM image shown in Fig. 6(c) agrees well with the SEM data. In addition, Fig. 6(b) reveals that the molten salt synthesis of BTO nanowire using $Ba(CH_3COO)_2$ as the precursor.

In spite of some trace spherical particles, the rods are long, and the diameters vary from several nanometers to ~500 nm. The SAED pattern indicates that the growth direction of BTO nanowires is along its *c*-axis. It is assumed that the as-synthesized perovskite crystal nanoseeds in the molten salt would arrange in a certain way to reduce the surface energy of the fresh section. After that, more and more crystals would aggregate and combine with the initially formed nanostructures along the self-polarized *c* direction, *i.e.*, the growth direction [29]. The TEM image shown in Fig. 6(d) also agrees with the BTO nanowire image shown in Fig. 6(b).

3.3. KNN nanocrystals

Table 2 lists the synthesis key words and references of some niobate-based, 1D nanomaterials. The hydrothermal method, molten salt reaction and some other synthesis approaches are introduced in detail with related description of the studies.

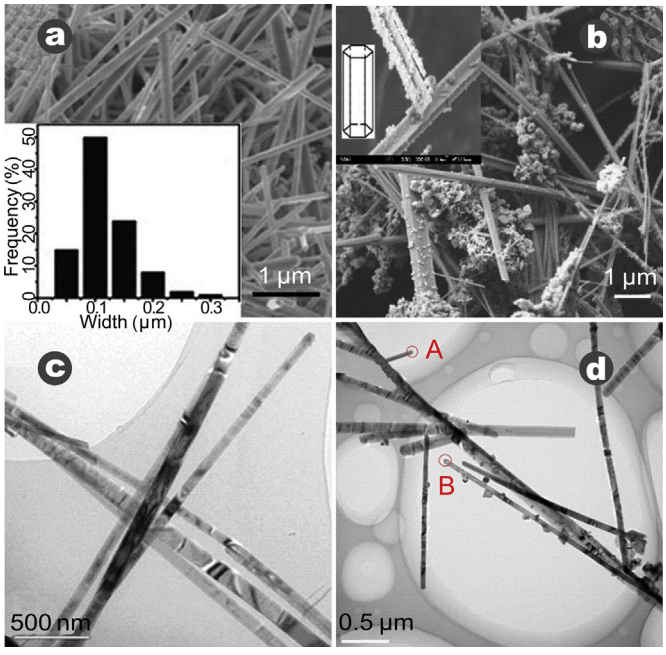

Fig. 6. BTO nanorod fabricated by molten salt method. (a) SEM image of BTO nanorod together with the statistic of width [50]. (b) SEM result of as-synthesized BTO nanowire and one enlarged image of one rod as the inset [29]. (c) and (d) TEM images of 1D BTO nanostructures corresponding to the rod shown in (a) [50] and (b) [29], respectively.

Table 2
List of the synthesis of one dimensional niobate based nanocrystals.

Products	Description	Reference
Hydrothermal method		
$NaNbO_3$	100 nm in diameter; NaOH solution adjustment; piezoelectricity determination	[61]
$KNbO_3$	Temperature–pressure condition variation; a narrow window of diagram of $KOH–Nb_2O_5–H_2O$; structure transformation	[62]
	Polymorphous nanocrystals; low temperature	[63]
$LiNbO_3$	SHG signal measurement; DEP response	[64]
$K_{1-x}Na_xNbO_3$	Phase structure change with composition; Raman study; UV/vis absorption study;	[65]
Molten salt method		
$NaNbO_3$	Topochemical method; Nb_2O_5 precursor	[66]
	Ion exchange; $K_2Nb_8O_{21}$ precursor	[67]
$KNbO_3$	Topochemical method; Nb_2O_5 precursor	[66]
	Three kinds of precursors; preferential orientation of the crystals	[68]
$K_{1-x}Na_xNbO_3$	Topochemical method; Nb_2O_5 precursor; ceramic preparation	[66]
	Different precursors; preferential orientation of the crystals	[68]
	Structure transformation; piezoelectricity characterization; composition measurement	[35,38]
Other methods		
$LiNbO_3$	Nanotube; ordered alumina template	[69]
	Decomposition; reaction of alkoxide precursor and triphenylphosphine oxide	[70]
$NaNbO_3$	Decomposition; niobium oxooxalate complex	[71]
	$In_2O_3/NaNbO_3$; co-precipitation method	[72]
	Gel precursor; templated crystallization	[73]

KNN-based 1D nanomaterials have been highly focused due to the high piezoelectric performance, and the molten salt method is increasingly used for their synthesis. Actually, the molten salt method was employed several decades ago for the synthesis of $BaFe_{12}O_{19}$ and $SrFe_{12}O_{19}$ crystals as reported by Arendt [74]. PZT materials based on molten-salt solvent were synthesized as powders in 1979 [75]. Since then, the molten salt method has become attractive for producing highly crystallized, size-controlled nanostructures [6]. Chiu et al. also reported the fabrication of complex perovskite $Pb(Fe_{0.5}Nb_{0.5})O_3$ [76].

For the synthesis of 1D nanocrystals by molten salt method, the key reaction step is the formation of 1D precursors whose morphology will be inherited finally by the targeted perovskite

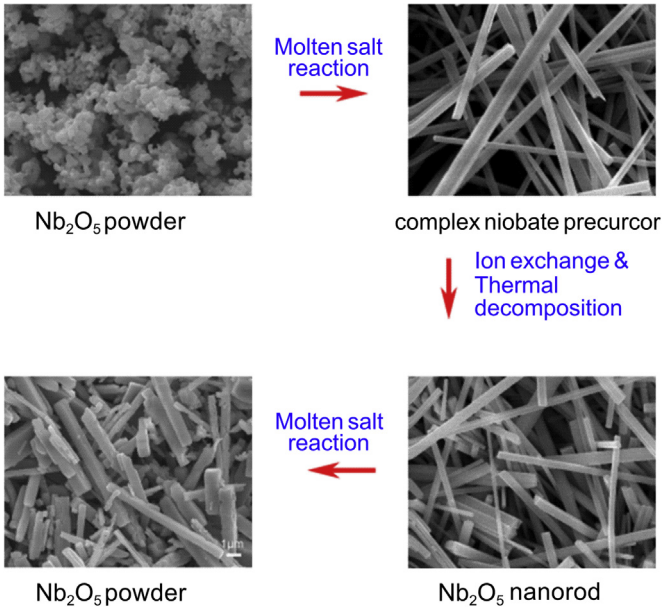

Fig. 7. Flow chart of synthesis reactions and products for the molten reaction synthesis of KNN nanorods.

crystals [66]. For example, Xu et al. reported a complex niobate precursor synthesis of $NaNbO_3$ and $Ca(NbO_3)_2$ NRs, and the products were both well crystallized [67]. Madaro et al. revealed the chemical conversion of $KNbO_3$ and $K_{0.5}Na_{0.5}NbO_3$ single crystals from various complex niobate precursors [68]. The perovskite niobate nanostructures are anisometric, and their morphology is highly dependent on that of complex niobate precursors such as needle-like $K_2Nb_4O_{11}$, long plate-like KNb_3O_8 and $K_4Nb_6O_{17}\cdot 3H_2O$ plate particles [68]. Xing's group extensively studied the synthesis of niobate nanostructures in both nanowires and micron-platelet particles, and also fabricated complex niobate based products with 1D and plate-like morphology as precursors [66,77,78]. Santulli et al. also reported the synthesis of $LiNbO_3$ NRs from the same 1D niobate precursor [79].

Based on these studies, the molten salt synthesis of KNN nanorods consists of four steps (Fig. 7) with the evolution of products morphology. The equiaxed Nb_2O_5 particles first convert to complex niobate precursors with high aspect ratio *via* a molten salt reaction that is the initial precursor. After that, the high-aspect-ratio nanorods act as templates for the formation of Nb_2O_5 nanorods. The Nb_2O_5 nanorods obtained *via* ion exchange and thermal decomposition processes inherit the morphology of the smooth surface and length, which is typically tens of micrometers.

$$2H_3ONb_3O_8 \rightarrow 3Nb_2O_5 + 3H_2O$$

Finally, the Nb_2O_5 nanorods, together with appropriate reactants, transform to KNN NRs *via* the molten salt reaction according to:

$$Nb_2O_5 + xK_2CO_3 + (1-x)Na_2CO_3 \xrightarrow{KCl} 2K_xNa_{1-x}NbO_3 + CO_2\uparrow$$

The as-synthesized KNN NRs reaches 10–20 μm in length and 400–500 nm wide.

The crystallographic evolution of the Nb-containing species during the synthesis of KNN nanorods is schematically shown in Fig. 8 [38]. The Nb atoms are located in the center of the oxygen-octahedra. The anions of complex niobate products have a framework based on the tetragonal bronze structure; most Nb atoms occupy octahedral, and the others are triangular tunnels and share NbO_6 octahedra on the corners. The complex niobate precursor then transforms into the $H_3ONb_3O_8$ structures. This complex compound is further converted back into niobium pentoxide, which inherits NR morphology and exhibits a corner- and edge-shared NbO_6 octahedra network. Thus, all of these efforts are devoted to changing Nb_2O_5 from equiaxial morphology to high-aspect-ratio nanorods. This serves as a template for the KNN nanorod synthesis through the molten-salt reaction. Finally, the network transforms to a corner-sharing perovskite structure [78,80].

The SEM and TEM images of the representative KNN nanorods synthesized by molten salt reaction are displayed in Fig. 9 [36,38,66]. Fig. 9(a) and (b) show the morphology of KNN nanorods and reveal that the diameters of the KNN nanorods range from 200 to 700 nm with lengths of 10–20 μm [36,80]. The morphology is similar to titanate nanowires [81,82]. The enlarged SEM image for an individual nanorod is shown in Fig. 9(c). The surface of the rod is smooth and the diameter varies somewhat along the length of the NR. The top-view image in Fig. 9(c) is nearly square. Meanwhile, the

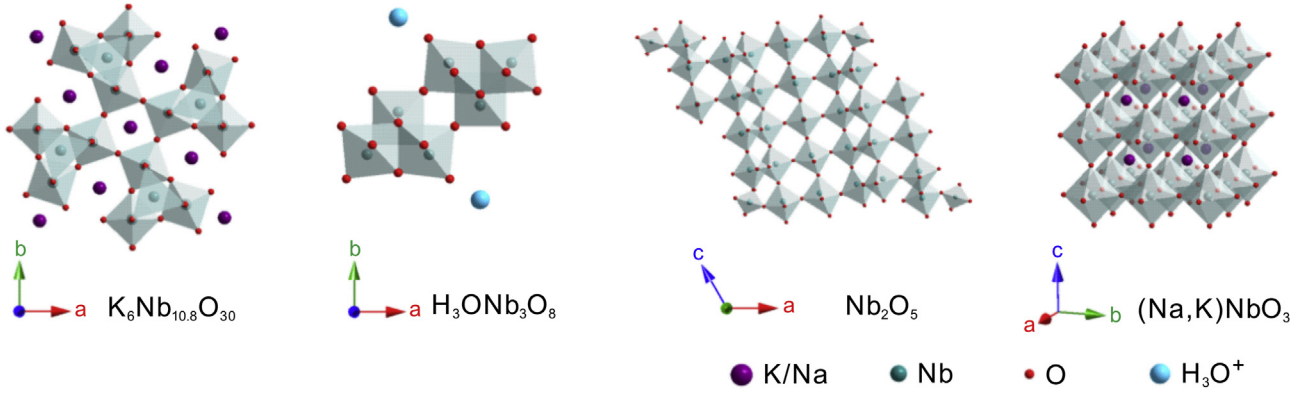

Fig. 8. Schematic illustration of the structure evolution of products obtained during the molten salt synthesis of KNN nanorods [38].

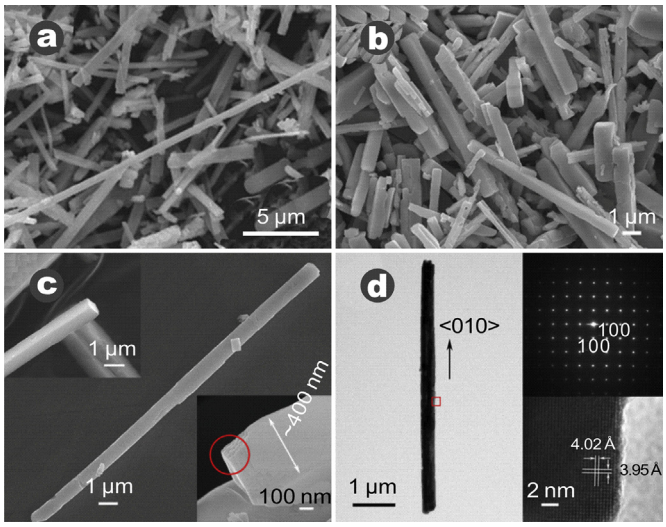

Fig. 9. KNN nanorods synthesized by molten salt reaction. (a) [80] and (b) [36] SEM images of KNN nanorods, (c) morphology of an individual KNN nanorod, and the top view of the tip of a representative nanorod, respectively, and (d) TEM image of nanorod together with SEAD pattern and HRTEM image [38].

nanoscale steps have heights of ~5–10 nm at the tip of an individual NR. These are marked with the red circle in Fig. 9(c). These steps might correspond to the growth stages [83] and provide evidence for growth mechanisms with preferential orientations [40,64,78]. The bright-field TEM images of the KNN nanorod are also presented in Fig. 9(d). They are consistent with the SEM results presented in Fig. 9(c). The single crystalline nature of KNN NRs is indicated according to plots of the selected area electron diffraction (SEAD) pattern [38] (For interpretation of the references to color in this paragraph, the reader is referred to the web version of this article.).

The single crystalline nature of KNN NRs is indicated according to plots of the SEAD pattern [38]. Different regions of the nanorod had the same SAED results indicating that the current KNN NR is single crystal with a growth direction in the ⟨010⟩. Moreover, the high-resolution transmission electron microscopy (HRTEM) data (Fig. 9(d)) shows interplanar spacing of 4.01 Å and 3.95 Å corresponding to the ⟨100⟩ and ⟨010⟩ directions, respectively. These are consistent with KNN bulk materials [84].

Hydrothermal synthesis is another approach to fabricate KNN 1D nanocrystals. In 2001, Cho et al. reported hydrothermal synthesis of acicular PZT structures, which paved the way of hydrothermal fabrication method in 1D piezoelectric perovskites [43]. Next, Liu et al. reported the successful synthesis of $KNbO_3$ NRs with hydrothermal synthesis in 2002 [63]. Since then, many research groups have published their syntheses and properties characterization of 1D piezoelectric nanostructures. Vasco et al. investigated the growth kinetic of 1D $KNbO_3$ nanostructures synthesized by a hydrothermal route. From this, a model was designed to account for the cube-based morphology of the nanostructures [83]. Wang et al. reported the synthesis of KNN nanostructures, analyzed the growth mechanism and optical properties in 2010 [65]. Furthermore, $K_xNa_{1-x}NbO_3$ nanorods were fabricated *via* a hydrothermal method that was accompanied by a post-heat treatment process [21].

The morphology and structure vary a lot at different temperatures and reaction times [85], even under the same reaction conditions [65,86]. Fig. 10(a) and (b) show KNN nanorods with different morphologies synthesized *via* a hydrothermal method. The data indicate that hydrothermal synthesis is a variable and intractable method [65,86]. In addition, the 1D nanostructures can also be synthesized as aligned arrays on a substrate. Xu et al. reported the fabrication of KNN NRs grown on different substrates, *i.e.* STO/KNN (100) ($SrTiO_3$/KNN) and STO/KNN (111) substrate as shown in Fig. 10(c) and (d) [40]. They used a special installation to hold the substrate as illustrated in Fig. 11. The growth of arrays takes place in the KNN film-coated STO substrate [40,53]. The substrate is mounted on the substrate holder, inverted, and soaked in a hydrothermal reaction solution. The distance from substrate the holder and the autoclave bottom can be controlled. This setup was first introduced in the synthesis of PT nanostructures by Rørvik et al. in 2009 [53]. This approach

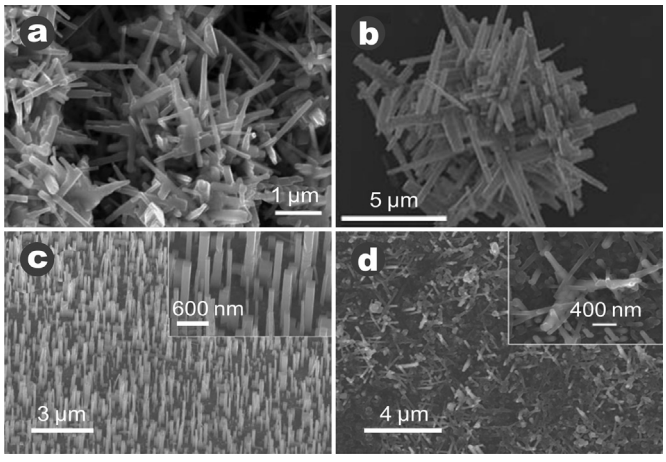

Fig. 10. KNN nanorods synthesized by hydrothermal. (a) $(K_{0.99}Na_{0.01})NbO_3$ nanorods synthesized at 220 °C for 24 h [86]. (b) $K_{0.50}Na_{0.50}NbO_3$ nanorods fabricated under 200 °C for 24 h [65]. (c) KNN nanorods on KNN/STO(100) substrates at 200 °C for 24 h [40]. (d) KNN nanorods on KNN/STO(111) substrates at 205 °C for 24 h [40].

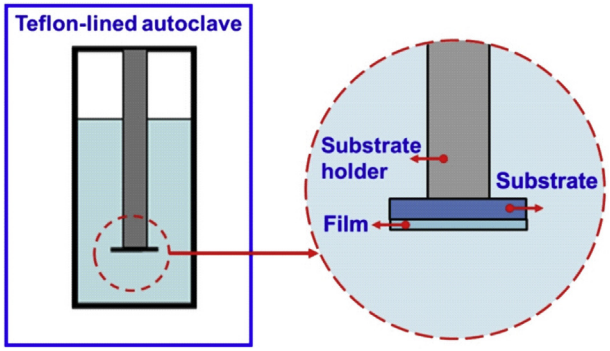

Fig. 11. Illustration of the experimental setup for the fabrication of aligned arrays synthesized by hydrothermal method.

is also effective in the synthesis of KNN nanorods grown on the substrate surface facing downward in the autoclave.

4. Piezoelectricity characterization

Compared with the traditional piezoelectric bulk materials, the characterization of piezoelectric crystals, especially the piezo-nanocrystal, is a critical problem because it is difficult to observe piezoelectric nanostructures at the nano/micro-scale. New research is establishing the relationship among the microstructure, piezoelectricity at the nanoscale and the performance of macro materials. Recently, the properties of 1D piezoelectric nanostructures were investigated with piezoresponse force microscopy (PFM) [23]. This is an effective technique for drawing topography and conducting nondestructive property characterization of piezoelectric and ferroelectric materials at the nanoscale. For instance, Kalinin's group developed a switching spectroscopy piezoresponse force microscopy (SS-PFM) to quantitatively address local switching characteristics of the PZT materials [87]. Moreover, piezoelectric properties of monocrystalline PZT nanowires, KNN nanorods and polycrystalline $BiFeO_3$ nanofibers were also investigated, respectively [36,88,89]. Even soft biological tissues were shown to be electromechanically coupled in porcine aortic walls and elastin [23,24,90].

Fig. 12 presents the morphology and piezoelectric performance measured by AFM and PFM, respectively. The AFM/PFM results of 1D PZT nanostructures are shown in Fig. 12(a)–(c) [88]. The topography presented in Fig. 12(a) was first drawn by the AFM tip. The amplitude (Fig. 12(b) left) and phase (Fig. 12(b) right) are related to piezoelectric vibration and polarization. These were acquired concurrently. The piezoelectric response loop shown in Fig. 12(c) was obtained with a positive voltage cycle and reveals a typical piezoelectric hysteresis. Wang et al. studied the PFM characterization of BTO nanowires in both vertical and lateral modes [90]. Fig. 12(d) shows the morphology of the BTO nanowire, and lateral amplitude curves and phase hysteresis loops are revealed in Fig. 12(e) and (f), respectively. Our group conducted PFM study on the KNN NRs synthesized *via* molten-

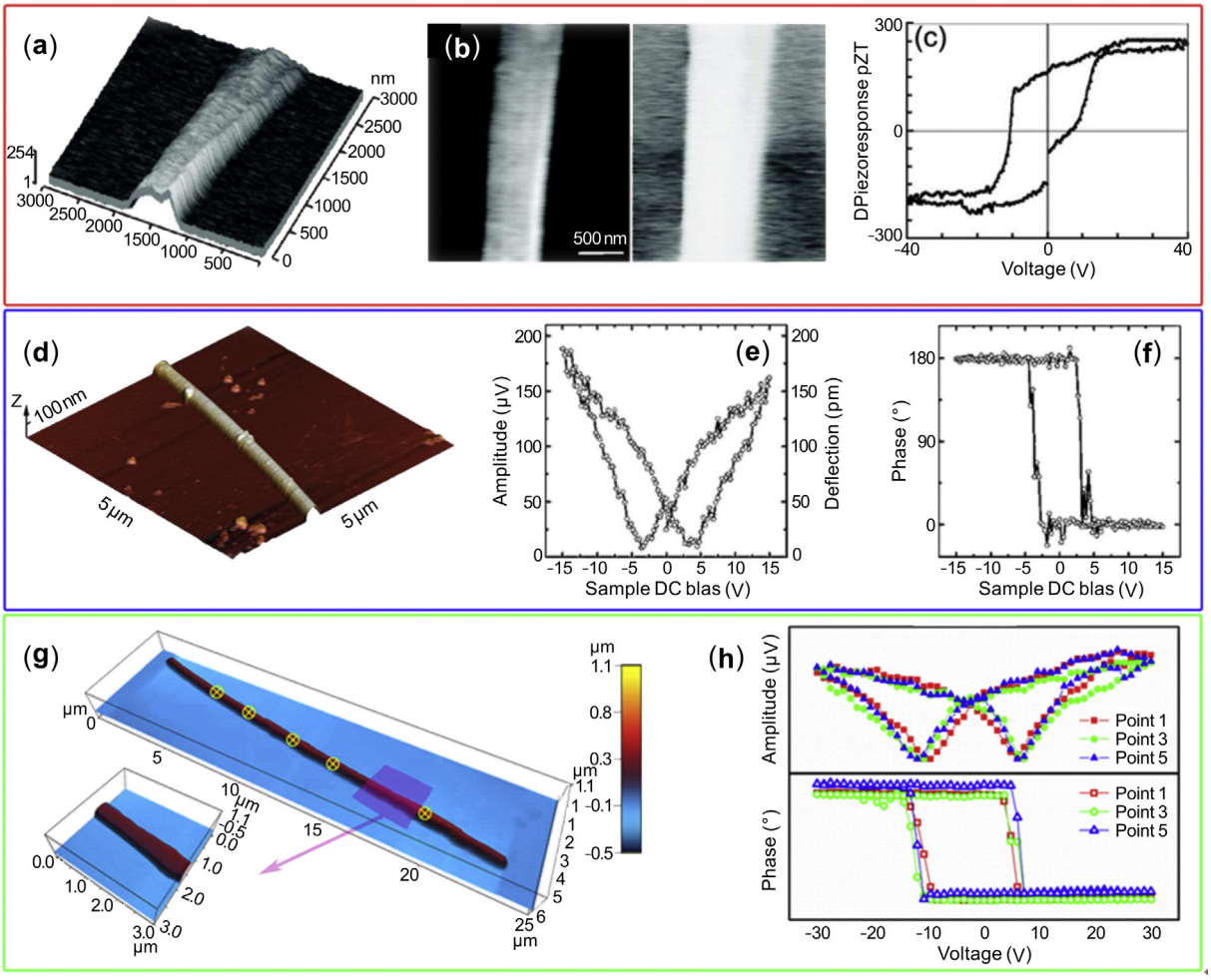

Fig. 12. AFM/PFM measurement of (a) PZT, (b) BTO and (c) KNN nanorods. (a) 3D drawing of the amplitude of PZT nanowire [88]. (b) The amplitude and phase information of PZT nanowire poled with voltage of −40 V applied on the bottom electrode [88]. (c) Local hysteresis loop of piezoresponse of PZT nanowire [88]. (d) AFM image of BTO nanowire [91]. Lateral PFM phase loop (e) and amplitude butterfly curve (f) of BTO nanowire [91]. (g) Morphology of the KNN nanorod [36]. (h) The piezoresponses and phase information obtained from three points as marked in (g) [36].

salt reaction [36]. Fig. 12(g) shows the AFM image of one individual NR ~25 μm in length and ~500–700 nm in width. Fig. 12(g) also indicates the measurement points that were set along the length direction. A sequence of DC voltage signals with "on" and "off" states in a periodic triangle wave. These were applied as shown in Fig. 12(c), and an AC signal was simultaneously applied to obtain the piezoelectric vibration [36]. Therefore, the amplitude butterfly curves and phase hysteresis loops were acquired, and the results are shown in Fig. 12(d) [24]. These results show the typical amplitude-voltage and phase-voltage hysteresis loops, respectively. They indicate the uniformity of the NRs. The phase boundary in KNN NRs was further confirmed by the composition dependence of piezoelectric responses [24,36,92].

5. Studies for piezoelectric applications

One dimensional piezoelectric nanostructure-based nanocomposites are a unique and interesting class of materials that synergize the advantages of piezoelectric nanomaterials and the polymer matrix. They have attracted extensive attention in applications of energy harvesting and self-powered sensing [93]. Most applications on 1D piezoelectric nanostructures includes sensors and nanogenerators for self-powered systems [49]. The size at the micro/nano scale renders the composite suitable for some personal electronic devices [94]. There are also many studies on 1D piezoelectric-based energy harvesting systems over the last decade. Wang's group has made great efforts in the fabrication and characterization of ZnO, as well as ZnO based composite [7,94,95]. However, the complex ternary piezoelectrics with perovskite (ABO_3) structure at low dimensions emerged during the past several years. It is reasonable that not only high piezoelectric performance but also multifunctional properties such as optical and magnetic properties exist in ABO_3 nanostructures [6,45]. Fig. 13 presents three illustrations of 1D piezomaterials based composites, including PZT, BTO, and $NaNbO_3$ nanowire systems.

The illustration of piezoelectric nanogenerators based on PZT nanofibers is shown in Fig. 13(a). The PZT nanofibers have a diameter and length of around 60 nm and 500 μm. These were aligned on interdigitated electrodes of platinum wires, respectively [96]. The output voltage and power under a periodic force was measured to be 1.63 V and 0.03 μW, respectively. Koka et al. reported the fabrication of a vertically aligned BTO nanowire array, and the energy harvesting behavior of the array was also evaluated [30]. The schematic drawing of the device is shown in Fig. 13(b). The device shown in Fig. 13(c) consists of $NaNbO_3$ nanowire-PDMS (polydimethylsilane) composite and Au/Cr-coated polymer films [97]. High-quality $NaNbO_3$ nanowires can be grown by a hydrothermal method at low temperature and poled by an electric field at room temperature. After that, the output voltage and current reach 3.2 V and 72 nA under a compressive strain, respectively. Recently, Wang et al. developed KNN nanofiber-based sensors with KNN nanofibers that were fabricated through electrospinning and polymer packaging process [98]. The composites exhibited a fast and active response that is proportional to the strain and generating rate.

However, there are still some unresolved issues with the flexible piezoelectric nanocomposites including insufficient output performance and size limitations before commercialization [99]. Specifically, the KNN-based piezoelectric nanostructures possess limited output voltage and current due to their relatively low piezoelectric coefficients [100]. Therefore, some other profound ways are highly desired in the fabrication of lead-free piezoelectric nanocomposites. Nanostructures with

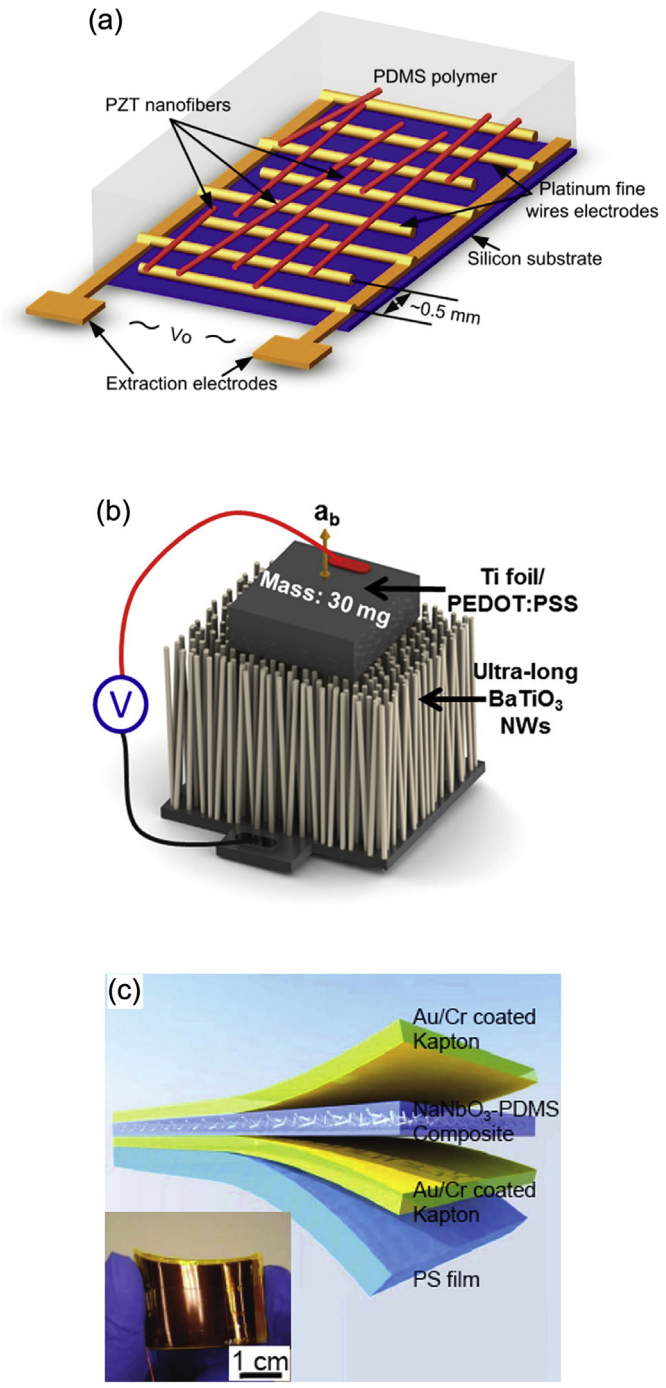

Fig. 13. Representative illustrations of composite systems based on 1D (a) PZT nanowire [96], (b) BTO nanowire [30], and (c) $NaNbO_3$ nanowire [97].

structure modifications and feature specialization including high-aspect-ratio nanorods, single crystal nanowires, *etc.* will likely have great potential for nanocomposites with large output signals. There are few reports of piezoelectric applications based on one dimensional KNN nanostuctures. Thus, more challenges and explorations are expected in this field.

6. Summary and outlook

The piezoelectric effect was discovered in 1880 by the Curie siblings and has been extensively studied and widely used in many technologies. Recently, one dimensional piezoelectric nanostructures are receiving extensive attention because of their promising applications in innovative technologies. In particular, 1D perovskite (ABO_3) nanocrystals are highly focused in the past two decades because of their multifunctional properties, *i.e.* ferroelectricity, high-temperature superconductivity, and colossal magnetoresistance. Thus, the 1D nanostructures with perovskite structure is a hot topic of interest not only for their potential applications but also for scientific interest and challenges.

Recently, there are three commonly studied research subjects based on 1D piezoelectric perovskite nanostructures. The first one is the controllable synthesis of perovskite nanostructures such as nanorods, nanowires, nanotubes, *etc.* In addition, aligned nanostructures grown on some substrates have also been investigated. Many studies have investigated the fabrication of 1D ABO_3 nanostructures, and the research interest is gradually developing single crystals due to the high piezoelectric performance. Secondly, emerging characterization techniques are also promoting the research of nanostructures. The measurement of nanostructures at the micro/nano-scale is beyond the traditional means of piezoelectric ceramics characterization. Ferroelectric and piezoelectric characterization along a special direction of the nanostructures is reasonably obtained because the test method is more microscopic. The last one could be referred as to the fabrication techniques of nanocomposites. The composites contain the 1D nanostructures as well as the polymer matrix and some other component. The composites are self-powered and could be utilized in energy harvesting systems, biomedical sensors and portable electronic devices.

In view of the recent research interest, we consider that the research focus in the near future would include the following two parts. First, academic research on 1D piezoelectric perovskite nanostructures should be emphasized. It is necessary to investigate the growth mechanism and effectively control the synthesis of perovskite nanostructures. Moreover, highly efficient syntheses of single crystalline nanostructures—along with ordered nanorod arrays—are expected. One dimensional single crystalline nanostructures are mostly fabricated *via* the molten salt and hydrothermal methods. However, the products are unstable versus conventional bulk piezomaterials. This makes the subsequent processing and fabrication of composites difficult. Second, novel structures with high output signals are expected. The composites will hopefully be based on lead-free piezoelectric nanomaterials. Certainly, more and more application studies based on 1D lead-free perovskite nanostructures are highly desired.

Acknowledgment

The authors acknowledge the financial supports from the National Natural Science Foundation of China (Grant No. 51332002) and the Ministry of Science and Technology of China (Grant No. 2015CB654605) as well as the State Key Laboratory of New Ceramics and Fine Processing Tsinghua University (Grant No. KF201512).

References

[1] Cross E. Lead-free at last. Nature 2004;432:24–5.
[2] Saito Y, Takao H, Tani T, Nonoyama T, Takatori K, Homma T, et al. Lead-free piezoceramics. Nature 2004;432:84–7.
[3] Li JF, Wang K, Zhu FY, Cheng LQ, Yao FZ. (K,Na)NbO_3-based lead-free piezoceramics: fundamental aspects, processing technologies, and remaining challenges. J Am Ceram Soc 2013;96:3677–96.
[4] Wang X, Wu J, Xiao D, Zhu J, Cheng X, Zheng T, et al. Giant piezoelectricity in potassium–sodium niobate lead-free ceramics. J Am Chem Soc 2014;136:2905–10.
[5] Shrout TR, Zhang SJ. Lead-free piezoelectric ceramics: alternatives for PZT? J Electroceram 2007;19:113–26.
[6] Rørvik PM, Grande T, Einarsrud MA. One-dimensional nanostructures of ferroelectric perovskites. Adv Mater 2011;23:4007–34.
[7] Wang X, Song J, Liu J, Wang ZL. Direct-current nanogenerator driven by ultrasonic waves. Science 2007;316:102–5.
[8] Wang ZL. Piezoelectric nanostructures: from growth phenomena to electric nanogenerators. MRS Bull 2007;32:109–16.
[9] Qin Y, Wang X, Wang ZL. Microfibre-nanowire hybrid structure for energy scavenging. Nature 2008;451:809–14.
[10] Zhou J, Fei P, Gao Y, Gu Y, Liu J, Bao G, et al. Mechanical-electrical triggers and sensors using piezoelectric micowires/nanowires. Nano Lett 2008;8:2725–30.
[11] Wu W, Cheng L, Bai S, Dou W, Xu Q, Wei Z, et al. Electrospinning lead-free 0.5Ba($Zr_{0.2}Ti_{0.8}$)O_3–0.5($Ba_{0.7}Ca_{0.3}$)TiO_3 nanowires and their application in energy harvesting. J Mater Chem A 2013;1:7332.
[12] Yi X, Li J. Synthesis and optical property of $NaTaO_3$ nanofibers prepared by electrospinning. J Sol-Gel Sci Technol 2009;53:480–4.
[13] McCann JT, Chen JIL, Li D, Ye ZG, Xia Y. Electrospinning of polycrystalline barium titanate nanofibers with controllable morphology and alignment. Chem Phys Lett 2006;424:162–6.
[14] Ávila HA, Ramajo LA, Góes MS, Reboredo MM, Castro MS, Parra R. Dielectric behavior of Epoxy/$BaTiO_3$ composites using nanostructured ceramic fibers obtained by electrospinning. ACS Appl Mat Interfaces 2013;5:505–10.
[15] Hossain M, Kim A. The effect of acetic acid on morphology of PZT nanofibers fabricated by electrospinning. Mater Lett 2009;63:789–92.
[16] Yoon KH, Cho YS, Kang DH. Molten salt synthesis of lead-based relaxors. J Mater Sci 1998;33:2977–84.
[17] Afanasiev P. Molten salt syntheses of alkali metal titanates. J Mater Sci 2006;41:1187–95.
[18] Zhan ZY, Xu CY, Zhen L, Wang WS, Shao WZ. Large-scale synthesis of single-crystalline KNb_3O_8 nanobelts via a simple molten salt method. Ceram Int 2010;36:679–82.
[19] Peng QX, Luo WB, Wu CG, Sun XY, Li P, Chen XY. The fabrication and pyroelectric properties of single crystalline PZT nanorod synthesized by hydrothermal reaction. J Mater Sci Mater Electron 2014;25:1627–32.
[20] Zhou Z, Lin Y, Tang H, Sodano HA. Hydrothermal growth of highly textured $BaTiO_3$ films composed of nanowires. Nanotechnology 2013;24.

[21] Xu H, Joung MR, Kim JS, Nahm S, Kang MG, Kang CY, et al. Synthesis of homogeneous $(Na_{1-x}K_x)NbO_3$ nanorods using hydrothermal and post-heat treatment processes. Chem Eng J 2012;211:16–21.
[22] Wang G, Selbach SM, Yu Y. Hydrothermal synthesis and characterization of $KNbO_3$ nanorods. CrystEngComm 2009;11:1958–63.
[23] Li J, Li JF, Yu Q, Chen QN, Xie S. Strain-based scanning probe microscopies for functional materials, biological structures, and electrochemical systems. J Materiomics 2015;1:3–21.
[24] Liu Y, Zhang Y, Chow MJ, Chen QN, Li J. Biological ferroelectricity uncovered in aortic walls by piezoresponse force microscopy. Phys Rev Lett 2012;108:078103.
[25] Park TJ, Mao YB, Wong SS. Synthesis and characterization of multiferroic $BiFeO_3$ nanotubes. Chem Commun 2004:2708–9.
[26] Wang XH, Chen RZ, Gui ZL, Li LT. The grain size effect on dielectric properties of $BaTiO_3$ based ceramics. Mater Sci Eng B 2003;99:199–202.
[27] Wang X, Deng X, Wen H, Li L. Phase transition and high dielectric constant of bulk dense nanograin barium titanate ceramics. Appl Phys Lett 2006;89:162902.
[28] Li Y, Liao Z, Fang F, Wang X, Li L, Zhu J. Significant increase of Curie temperature in nano-scale $BaTiO_3$. Appl Phys Lett 2014;105:182901.
[29] Li BR, Shang W, Hu ZL, Zhang NQ. Template-free fabrication of pure single-crystalline $BaTiO_3$ nano-wires by molten salt synthesis technique. Ceram Int 2014;40:73–80.
[30] Koka A, Zhou Z, Sodano HA. Vertically aligned $BaTiO_3$ nanowire arrays for energy harvesting. Energy Environ Sci 2014;7:288.
[31] Koka A, Zhou Z, Tang H, Sodano HA. Controlled synthesis of ultralong vertically aligned $BaTiO_3$ nanowire arrays for sensing and energy harvesting applications. Nanotechnology 2014;25.
[32] Tang H, Lin Y, Sodano HA. Synthesis of high aspect ratio $BaTiO_3$ nanowires for high energy density nanocomposite capacitors. Adv Energy Mater 2013;3:451–6.
[33] Joshi UA, Lee JS. Template-free hydrothermal synthesis of single-crystalline barium titanate and strontium titanate nanowires. Small 2005;1:1172–6.
[34] Wang K, Yao FZ, Jo W, Gobeljic D, Shvartsman VV, Lupascu DC, et al. Temperature-insensitive $(K,Na)NbO_3$-based lead-free piezoactuator ceramics. Adv Funct Mater 2013;23:4079–86.
[35] Cheng LQ, Wang K, Yu Q, Li JF. Structure and composition characterization of lead-free $(K, Na)NbO_3$ piezoelectric nanorods synthesized by the molten-salt reaction. J Mater Chem C 2014;2:1519.
[36] Cheng LQ, Wang K, Li JF, Liu Y, Li J. Piezoelectricity of lead-free $(K, Na)NbO_3$ nanoscale single crystals. J Mater Chem C 2014;2:9091–8.
[37] Yao FZ, Wang K, Li JF. Comprehensive investigation of elastic and electrical properties of Li/Ta-modified $(K,Na)NbO_3$ lead-free piezoceramics. J Appl Phys 2013;113:174105.
[38] Cheng LQ, Wang K, Li JF. Synthesis of highly piezoelectric lead-free $(K,Na)NbO_3$ one-dimensional perovskite nanostructures. Chem Commun 2013;49:4003–5.
[39] Zhou JJ, Li JF, Zhang XW. Orthorhombic to tetragonal phase transition due to stress release in (Li,Ta)-doped$(K,Na)NbO_3$ lead-free piezoceramics. J Eur Ceram Soc 2012;32:267–70.
[40] Xu Y, Li JF. A facile method to fabricate vertically aligned $(K,Na)NbO_3$ lead-free piezoelectric nanorods. J Mater Chem 2012;22:23221–6.
[41] Wang K, Li JF. Low-Temperature sintering of Li-modified $(K, Na)NbO_3$ lead-free ceramics: sintering behavior, microstructure, and electrical Properties. J Am Ceram Soc 2010;93:1101–7.
[42] Zhang XY, Zhao X, Lai CW, Wang J, Tang XG, Dai JY. Synthesis and piezoresponse of highly ordered $Pb(Zr_{0.53}Ti_{0.47})O_3$ nanowire arrays. Appl Phys Lett 2004;85:4190–2.
[43] Cho SB, Oledzka M, Riman RE. Hydrothermal synthesis of acicular lead zirconate titanate (PZT). J Cryst Growth 2001;226:313–26.
[44] Deng Y, Wang JL, Zhu KR, Zhang MS, Hong JM, Gu QR, et al. Synthesis and characterization of single-crystal $PbTiO_3$ nanorods. Mater Lett 2005;59:3272–5.
[45] Rørvik PM, Almli A, van Helvoort ATJ, Holmestad R, Tybell T, Grande T, et al. $PbTiO_3$ nanorod arrays grown by self-assembly of nanocrystals. Nanotechnology 2008;19.
[46] Alkoy EM, Dagdeviren C, Papila M. Processing conditions and aging effect on the morphology of PZT electrospun nanofibers, and dielectric properties of the resulting 3-3 PZT/polymer composite. J Am Ceram Soc 2009;92:2566–70.
[47] Lin Y, Liu Y, Sodano HA. Hydrothermal synthesis of vertically aligned lead zirconate titanate nanowire arrays. Appl Phys Lett 2009;95:122901.
[48] Bai S, Xu Q, Gu L, Ma F, Qin Y, Wang ZL. Single crystalline lead zirconate titanate (PZT) nano/micro-wire based self-powered UV sensor. Nano Energy 2012;1:789–95.
[49] Wu W, Bai S, Yuan M, Qin Y, Wang ZL, Jing T. Lead zirconate titanate nanowire textile nanogenerator for wearable energy-harvesting and self-powered devices. Acs Nano 2012;6:6231–5.
[50] Deng H, Qiu Y, Yang S. General surfactant-free synthesis of $MTiO_3$ (M = Ba, Sr, Pb) perovskite nanostrips. J Mater Chem 2009;19:976–82.
[51] Xu G, Ren ZH, Du PY, Weng WJ, Shen G, Han GR. Polymer-assisted hydrothermal synthesis of single-crystalline tetragonal perovskite $PbZr_{0.52}Ti_{0.48}O_3$ nanowires. Adv Mater 2005;17:907–10.
[52] Hu Y, Gu H, Hu Z, Di W, Yuan Y, You J, et al. Controllable hydrothermal synthesis of $KTa_{1-x}Nb_xO_3$ nanostructures with various morphologies and their growth mechanisms. Cryst Growth Des 2008;8:832–7.
[53] Rørvik PM, Grande T, Einarsrud MA. Hierarchical $PbTiO_3$ nanostructures grown on $SrTiO_3$ substrates. Cryst Growth Des 2009;9:1979–84.
[54] Gong W, Li JF, Peng CE, Gui ZL, Li LT. In-plane aligned $Pb(Zr_xTi_{1-x})O_3$ microbelts fabricated by near migration and restricted growth. Adv Mater 2005;17:1952–6.
[55] Urban JJ, Spanier JE, Lian OY, Yun WS, Park H. Single-crystalline barium titanate nanowires. Adv Mater 2003;15:423–6.
[56] Wang Y, Xu G, Yang L, Ren Z, Wei X, Weng W, et al. Hydrothermal synthesis of single-crystal $BaTiO_3$ dendrites. Mater Lett 2009;63:239–41.
[57] Joshi UA, Yoon SH, Baik SG, Lee JS. Surfactant-free hydrothermal synthesis of highly tetragonal barium titanate nanowires: a structural investigation. J Phys Chem B 2006;110:12249–56.
[58] Tang H, Zhou Z, Sodano HA. Relationship between $BaTiO_3$ nanowire aspect ratio and the dielectric permittivity of nanocomposites. ACS Appl Mater Interfaces 2014;6:5450–5.
[59] Zhou Z, Tang H, Sodano HA. Vertically aligned arrays of $BaTiO_3$ nanowires. ACS Appl Mater Interfaces 2013;5:11894–9.
[60] Mao YB, Banerjee S, Wong SS. Large-scale synthesis of single-crystal line perovskite nanostructures. J Am Chem Soc 2003;125:15718–9.
[61] Ke TY, Chen HA, Sheu HS, Yeh JW, Lin HN, Lee CY, et al. Sodium niobate nanowire and its piezoelectricity. J Phys Chem C 2008;112:8827–31.
[62] Magrez A, Vasco E, Seo JW, Dieker C, Setter N, Forro L. Growth of single-crystalline $KNbO_3$ nanostructures. J Phys Chem B 2006;110:58–61.
[63] Liu JF, Li XL, Li YD. Novel synthesis of polymorphous nanocrystalline $KNbO_3$ by a low temperature solution method. J Nanosci Nanotechnol 2002;2:617–9.
[64] Grange R, Choi JW, Hsieh CL, Pu Y, Magrez A, Smajda R, et al. Lithium niobate nanowires synthesis, optical properties, and manipulation. Appl Phys Lett 2009;95:143105.
[65] Wang Z, Gu H, Hu Y, Yang K, Hu M, Zhou D, et al. Synthesis, growth mechanism and optical properties of $(K,Na)NbO_3$ nanostructures. CrystEngComm 2010;12:3157–62.
[66] Li L, Deng J, Chen J, Sun X, Yu R, Liu G, et al. Wire structure and morphology transformation of niobium oxide and niobates by molten salt synthesis. Chem Mater 2009;21:1207–13.
[67] Xu CY, Zhen L, Yang R, Wang ZL. Synthesis of single-crystalline niobate nanorods via ion-exchange based on molten-salt reaction. J Am Chem Soc 2007;129:15444–5.
[68] Madaro F, Tolchard JR, Yu YD, Einarsrud MA, Grande T. Synthesis of anisometric $KNbO_3$ and $K_{0.5}Na_{0.5}NbO_3$ single crystals by chemical conversion of non-perovskite templates. CrystEngComm 2011;13:1350–9.
[69] Zhao LL, Steinhart M, Yosef M, Lee SK, Schlecht S. Large-scale template-assisted growth of $LiNbO_3$ one-dimensional nanostructures for nano-sensors. Sens Actuators B 2005;109:86–90.

[70] Wood BD, Mocanu V, Gates BD. Solution-phase synthesis of crystalline lithium niobate nanostructures. Adv Mater 2008;20:4552–6.
[71] Saito K, Kudo A. Niobium-complex-based syntheses of sodium niobate nanowires possessing superior photocatalytic properties. Inorg Chem 2010;49:2017–9.
[72] Lv J, Kako T, Li Z, Zou Z, Ye J. Synthesis and photocatalytic activities of $NaNbO_3$ rods modified by In_2O_3 nanoparticles. J Phys Chem C 2010; 114:6157–62.
[73] Pribošič I, Makovec D, Drofenik M. Formation of nanoneedles and nanoplatelets of $KNbO_3$ perovskite during templated crystallization of the precursor gel. Chem Mater 2005;17:2953–8.
[74] Arendt RH. Molten-salt synthesis of single magnetic domain $BaFe_{12}O_{19}$ and $SrFe_{12}O_{19}$ crystals. J Solid State Chem 1973;8:339–47.
[75] Arendt RH, Rosolowski JH, Szymaszek JW. Lead zirconate titanate ceramics from molten-salt slovent synthesized powders. Mater Res Bull 1979;14:703–9.
[76] Chiu CC, Li CC, Desu SB. Molten-salt synthesis of a complex perovskite $Pb(Fe_{0.5}Nb_{0.5})O_3$. J Am Ceram Soc 1991;74:38–41.
[77] Li L, Chen J, Deng A, Yu R, Qiao L, Liu G, et al. Topochemical synthesis of micron-platelet $(Na_{0.5}K_{0.5})NbO_3$ particles. Eur J Inorg Chem 2008:2186–90.
[78] Li L, Deng J, Yu R, Chen J, Wang X, Xing X. Phase evolution in low-dimensional niobium oxide synthesized by a topochemical method. Inorg Chem 2010;49:1397–403.
[79] Santulli AC, Zhou H, Berweger S, Raschke MB, Sutter E, Wong SS. Synthesis of single-crystalline one-dimensional $LiNbO_3$ nanowires. CrystEngComm 2010;12:2675–8.
[80] Xu S, Li JF. Synthesis and piezoelectricity of single-crystalline (K,Na) NbO_3 nanobars. J Am Ceram Soc 2011;94:3812–8.
[81] Huang KC, Huang TC, Hsieh WF. Morphology-controlled synthesis of barium titanate nanostructures. Inorg Chem 2009;48:9180–4.
[82] Xu CY, Zhang Q, Zhang H, Zhen L, Tang J, Qin LC. Synthesis and characterization of single-crystalline alkali titanate nanowires. J Am Chem Soc 2005;127:11584–5.
[83] Vasco E, Magrez A, Forró L, Setter N. Growth kinetics of one-dimensional $KNbO_3$ nanostructures by hydrothermal processing routes. J Phys Chem B 2005;109:14331–4.
[84] Zhang BP, Li JF, Wang K, Zhang HL. Compositional dependence of piezoelectric properties in $Na_xK_{1-x}NbO_3$ lead-free ceramics prepared by spark plasma sintering. J Am Ceram Soc 2006;89:1605–9.
[85] Joung MR, Xu H, Kim JS, Seo IT, Nahm S, Kang JY, et al. Structural variation of hydrothermally synthesized $KNbO_3$ nanowires. J Appl Phys 2012;111:114314.
[86] Sun C, Xing X, Chen J, Deng J, Li L, Yu R, et al. Hydrothermal synthesis of single crystalline (K,Na)NbO_3 powders. Eur J Inorg Chem 2007:1884–8.
[87] Kalinin SV, Gruverman A, Rodriguez BJ, Shin J, Baddorf AP, Karapetian E, et al. Nanoelectromechanics of polarization switching in piezoresponse force microscopy. J Appl Phys 2005;97:074305.
[88] Wang J, Sandu CS, Colla E, Wang Y, Ma W, Gysel R, et al. Ferroelectric domains and piezoelectricity in monocrystalline $Pb(Zr,Ti)O_3$ nanowires. Appl Phys Lett 2007;90:133107.
[89] Xie SH, Gannepalli A, Chen QN, Liu YM, Zhou YC, Proksch R, et al. High resolution quantitative piezoresponse force microscopy of $BiFeO_3$ nanofibers with dramatically enhanced sensitivity. Nanoscale 2012;4: 408–13.
[90] Liu YM, Wang YJ, Chow MJ, Chen NQ, Ma FY, Zhang YH, et al. Glucose suppresses biological ferroelectricity in aortic elastin. Phys Rev Lett 2013;110:168101.
[91] Wang Z, Hu J, Yu MF. One-dimensional ferroelectric monodomain formation in single crystalline $BaTiO_3$ nanowire. Appl Phys Lett 2006; 89:263119.
[92] Chen QN, Ma F, Xie S, Liu Y, Proksch R, Li J. High sensitivity piezomagnetic force microscopy for quantitative probing of magnetic materials at the nanoscale. Nanoscale 2013;5:5747–51.
[93] Yang Y, Jung JH, Yun BK, Zhang F, Pradel KC, Guo W, et al. Flexible pyroelectric nanogenerators using a composite structure of lead-free $KNbO_3$ nanowires. Adv Mater 2012;24:5357–62.
[94] Zhu G, Yang R, Wang S, Wang ZL. Flexible high-output nanogenerator based on lateral ZnO nanowire array. Nano Lett 2010;10: 3151–5.
[95] Mantini G, Gao Y, D'Amico A, Falconi C, Wang ZL. Equilibrium piezoelectric potential distribution in a deformed ZnO nanowire. Nano Res 2009;2:624–9.
[96] Chen X, Xu S, Yao N, Shi Y. 1.6 V nanogenerator for mechanical energy harvesting using PZT nanofibers. Nano Lett 2010;10: 2133–7.
[97] Jung JH, Lee M, Hong JI, Ding Y, Chen CY, Chou LJ, et al. Lead-free $NaNbO_3$ nanowires for a high output piezoelectric nanogenerator. Acs Nano 2011;5:10041–6.
[98] Wang Z, Zhang Y, Yang S, Hu Y, Wang S, Gu H, et al. (K,Na)NbO_3 nanofiber-based self-powered sensors for accurate detection of dynamic strain. ACS Appl Mater Interfaces 2015;7:4921–7.
[99] Park K-I, Jeong CK, Ryu J, Hwang G-T, Lee KJ. Flexible and large-area nanocomposite generators based on lead zirconate titanate particles and carbon nanotubes. Adv Energy Mater 2013:1539–44.
[100] Xu SY, Yeh YW, Poirier G, McAlpine MC, Register RA, Yao N. Flexible piezoelectric PMN-PT nanowire-based nanocomposite and device. Nano Lett 2013;13:2393–8.

Li-Qian Cheng is currently a lecturer of China University of Mining & Technology, Beijing, China. She received her B.E. degree in Materials Science and Engineering from Central South University, Changsha, China, in 2010. Afterward, she joined the Prof. Jing-Feng Li's group in the State Key Laboratory of New Ceramics and Fine Processing in Tsinghua University. She received her Ph.D. Degree in the School of Materials Science and Engineering, Tsinghua University, Beijing, China. In 2015, she became a faculty member in China University of Mining & Technology, Beijing. Her research interests include the synthesis and characterizations of low dimensional piezoelectric nanostructures and bulk ceramics.

Jing-Feng Li is a "Changjiang Scholar" distinguished professor of Materials Science and Engineering at Tsinghua University. He has received master and doctor degrees both from Tohoku University (Japan) in 1988 and 1991, and a Bachelor of Engineering from Huazhong University of Science and Technology, China, in 1984. After working in Tohoku University as an assistant professor from 1992 to 1997, and an associate professor from 1997 to 2002, Prof. Li joined Tsinghua University as a full professor in 2002. His research interests include piezoelectric ceramics and composites, piezoelectric films for MEMS applications, thermoelectric materials and microdevices, materials microfabrication. Prof. Li is an Editor-in-Chief of Journal of Materioimics, Associate editor of Journal of Chinese Ceramic Society, and also a member of editorial board for several international journals. He also was an associated editor and subject editor for Journal of Materials Processing Technology from 2005 to 2013. He authored/co-authored >330 papers and 34 patents as well as two books, delivered 50+ invited/keynote talks in international conferences, and received several awards including young researcher award from the Japan Institute of Metals and outstanding young scientist grant from NSF of China.